Drag force in bimodal cubic-quintic nonlinear Schrödinger equation

David Feijoo, Ismael Ordóñez, Angel Paredes, and Humberto Michinel

Área de Óptica, Departamento de Física Aplicada, Universidade de Vigo, As Lagoas s/n, Ourense ES-32004, Spain

We consider a system of two cubic-quintic nonlinear Schrödinger equations in two dimensions, coupled by repulsive cubic terms. We analyze situations in which a probe lump of one of the modes is surrounded by a fluid of the other one and analyze their interaction. We find a realization of D'Alembert's paradox for small velocities and nontrivial drag forces for larger ones. We present numerical analysis including the search of static and traveling form-preserving solutions along with simulations of the dynamical evolution in some representative examples.

I. INTRODUCTION

The nonlinear Schrödinger equation (NLSE) is a widely used model in the study of quasimonochromatic, nonlinear dispersive waves. Among other applications, it describes the dynamics of Bose-Einstein condensates (BECs) in the mean field approximation [1] or the propagation of laser beams in optical fibers [2], for which different expressions have been used for the nonlinearity of the refractive index [3]. The cubic-quintic NLSE [4] is arguably the simplest model for competing nonlinearities [5] and has been used in many different contexts; see, e.g., Refs. [6–9], and references therein. In two transverse dimensions, which is a relevant case for nonlinear optics, the cubic (focusing)-quintic (defocusing) model (CQNLSE) presents remarkable features. There are families of stable solitary waves (solitons and vortices) which become flattop when the power of the beam is large: the propagation constant never exceeds a critical value β_{cr}, and, for growing power $\beta \to \beta_{cr}^-$, there is a growing region where the amplitude also tends to a critical value $\psi \approx e^{i\beta_{cr}z}\psi_{cr}$, as was established by different numerical and analytical methods in Ref. [10] and later rigorously proved in Ref. [8]. It is worth remarking the similarity with results found in the study of the complex cubic-quintic system in which linear and nonlinear loss and gain terms are included; see Ref. [11], and references therein. This model is used in the description of the generation of ultrashort pulses in certain mode-locked laser oscillators.

The aforementioned behavior endows the flattop solutions of the CQNLSE with the properties of a liquid [12]. The $|\psi| \approx \psi_{cr}$ is a region of constant pressure, and the rapid decay from $|\psi| \approx \psi_{cr}$ to $|\psi| \approx 0$ can be identified with a liquid-vapor interface characterized by a surface tension, leading to effects analogous to capillarity and dripping in regular liquids [13]. Remarkably, the first neat experimental realization of this liquid of light has been reported recently [14], following the proposal of engineering the desired optical properties in a coherent medium [15].

A natural question is whether there are other hydrodynamical properties that can be defined for this kind of solutions of the CQNLSE. In this paper we analyze the drag, namely, the force which opposes to the motion of an object within a surrounding fluid. An "object" inside the fluid described by a NLSE can be modeled by implementing appropriate boundary conditions at the edge of the moving body, as was done in the framework of superfluidity in Refs. [7,16], where similar questions to those addressed here were studied. We

will consider a different approach which might be suitable for nonlinear optics or BECs: the probe object is also described by a CQNLSE, leading to a bimodal system of coupled equations for two wave functions ψ_1, ψ_2. In nonlinear optics [17], the ψ_n typically correspond to different polarizations or different carrier wavelengths, while in BECs they represent different atomic species in the condensate [18] or different internal states of the same isotope [19]; see, e.g., Ref. [20], and references therein.

The system of equations we will study is the following:

$$-i\partial_z\psi_1 = \nabla^2\psi_1 + (|\psi_1|^2 - |\psi_1|^4 - \gamma |\psi_2|^2)\psi_1,$$
$$-i\partial_z\psi_2 = \nabla^2\psi_2 + (|\psi_2|^2 - |\psi_2|^4 - \gamma |\psi_1|^2)\psi_2, \quad (1)$$

where for simplicity we have fixed to unity several coefficients. The Laplacian is taken over two transverse dimensions $\nabla^2 = \partial_x^2 + \partial_y^2$. For the crossed interaction, we only introduce cubic terms weighed by a constant γ. Being the most suitable situation to formulate thought experiments regarding drag forces, we will restrict ourselves to analyzing $\gamma > 0$, namely, inter-modal repulsion resulting in a fluid with immiscible phases. Even if the specific choice of the form of the crossed terms in Eq. (1) is somewhat arbitrary, it is sufficient to explore the general behavior of bimodal cubic-quintic systems of this sort.

A bimodal cubic-quintic model similar to (1) was first introduced in Ref. [21] to discuss the interaction between solitons of both species. Variations of this model were later used for the study of vector solitons [22], their dynamics [23], and modulational instability [24,25]. It is worth pointing out that these works mostly deal with intermodal attraction $\gamma < 0$. An exception is Ref. [25], which deals with BECs where interspecies forces can be tuned using Feshbach resonances and can be either attractive or repulsive.

In Eqs. (1), the norm $\int |\psi_n|^2 dx\, dy$ for each species is conserved separately upon evolution in z. Moreover, it is straightforward to check that total momentum is preserved:

$$\vec{p} = \frac{1}{2i} \int \sum_{n=1,2} (\psi_n^*\vec{\nabla}\psi_n - \psi_n\vec{\nabla}\psi_n^*)dx\, dy, \quad (2)$$

but the $\vec{p}_n$ associated to each species are not separately conserved, i.e., momentum can be transferred between species, leading to intermodal macroscopic forces. In the following, we will consider the dynamics of a droplet of ψ_1 surrounded by a large background of ψ_2, with $\int |\psi_2|^2 dS \gg \int |\psi_1|^2 dS$. We

thus study the effects of the drag force exerted by the ψ_2 fluid on an ψ_1 probe "object."

In Sec. II we discuss the static solutions. In Sec. III we find form-preserving traveling solutions which can be interpreted as dragless motion of an object within an inviscid fluid and are therefore related to D'Alembert's paradox. These configurations exist below some limiting velocity. We also discuss how this kind of solutions can be approached in processes with dynamical evolution. In Sec. IV we devise a kind of thought falling ball viscometer experiment and introduce an approximate analogy between this intricate nonlinear setup and a simple mechanical system. In Sec. V we consider a case in which both species are initially separated and show the similarity of simulated processes with the entrance of a rigid object in a liquid. Finally, we present our conclusions in Sec. VI.

II. STATIC SOLUTIONS

We start by looking for radially symmetric, stationary solutions with a circle of ψ_1 surrounded by an infinite critical background of ψ_2, with $\int |\psi_2|^2 \, dS = \infty$, namely,

$$\psi_1 = e^{i\,\beta_1 z} f_1(r), \quad \psi_2 = e^{i\,\beta_{cr} z} f_2(r), \tag{3}$$

where $f_1(r)$, $f_2(r)$ are real functions and $\beta_{cr} = \frac{3}{16}$ [8]. The system (1) is reduced to

$$
\begin{aligned}
\partial_r^2 f_1 + r^{-1}\partial_r f_1 &= \beta_1 f_1 - \left(f_1^2 - f_1^4 - \gamma f_2^2\right) f_1, \\
\partial_r^2 f_2 + r^{-1}\partial_r f_2 &= \beta_{cr} f_2 - \left(f_2^2 - f_2^4 - \gamma f_1^2\right) f_2.
\end{aligned}
\tag{4}
$$

Boundary conditions at infinity are

$$\lim_{r \to \infty} f_1(r) = 0, \quad \lim_{r \to \infty} f_2(r) = \psi_{cr} = \sqrt{3}/2. \tag{5}$$

The profile of the functions at $r \to \infty$ consistent with (5) can be found by computing the leading terms in (4). We find that $f_1(r) \sim r^{-1/2} \exp(-\sqrt{\beta_1 + 3\gamma/4}\, r)$. Therefore, solutions can only exist for $-\frac{3}{4}\gamma < \beta_1$. The function f_2 behaves as $\sqrt{3}/2 - f_2(r) \sim r^{-1/2}\exp(-\sqrt{3}r/2)$ if $\beta_1 > \frac{3}{16}(1 - 4\gamma)$ and as $\sqrt{3}/2 - f_2(r) \sim \exp(-2\sqrt{\beta_1 + 3\gamma/4}\,r)$ for $\beta_1 \leqslant \frac{3}{16}(1 - 4\gamma)$.

At $r = 0$, solutions must be regular $f_1'(0) = f_2'(0) = 0$. By performing a Taylor expansion, we find that near the origin the functions can be written in terms of two constants:

$$f_1(r) = a_0 + \frac{a_0}{4}\left(\beta_1 - a_0^2 + a_0^4 + \gamma\, b_0^2\right)r^2 + O(r^4),$$

$$f_2(r) = b_0 + \frac{b_0}{4}\left(\frac{3}{16} - b_0^2 + b_0^4 + \gamma\, a_0^2\right)r^2 + O(r^4).$$

For a given γ, numerical solutions of (4) and (5) can be found by rewriting the equations in a finite differences scheme and solving the resulting nonlinear algebraic system by standard methods. The asymptotic expansions presented above give some evidence on the existence of the full solutions and are useful to cross-check that the numerical approximations match the analytical computations in both limits $r \to 0$ and $r \to \infty$. Figure 1 shows three examples of $f_1(r)$, $f_2(r)$ pairs computed numerically.

For a given γ, we find a one-parameter family of nodeless monotonic solutions [$f_1'(r) < 0$ and $f_2'(r) > 0$ $\forall r > 0$]. Thus, for fixed β_1 and γ there exists a single solution of the equations.
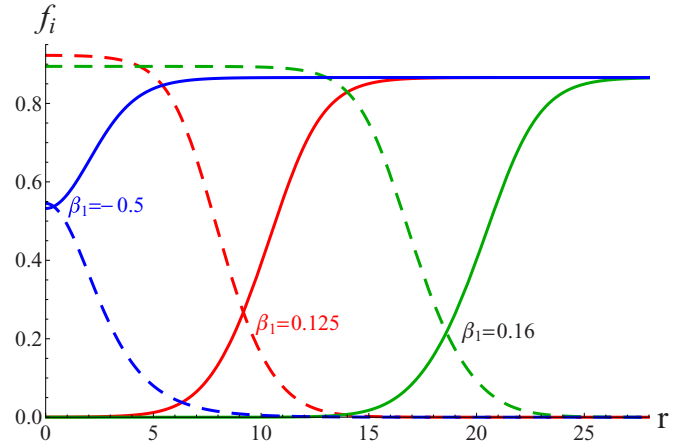
FIG. 1. (Color online) Solutions of (4) and (5) with $\gamma = 1$ for $\beta_1 = -0.5$, $\beta_1 = 0.125$, and $\beta_1 = 0.16$. For larger β_1, the value r_* at which $f_1(r)$ decays and $f_2(r)$ rises increases, and, therefore, the normalization $\int |\psi_1|^2 \, dS$ also grows. Dashed lines correspond to $f_1(r)$ and solid lines to $f_2(r)$.

In Fig. 2 we depict the values $f_1(0) = a_0$, $f_2(0) = b_0$ for the families of solutions with $\gamma = 1$ and $\gamma = 2$.

The parameter β_1 can take values in the interval $-\frac{3}{4}\gamma < \beta_1 < \frac{3}{16}$. When $\beta_1 \to -\frac{3}{4}\gamma$, we have $a_0 \to 0$ and $b_0 \to \sqrt{3}/2$, yielding a solution where, simply, $f_1(r) = 0$ and $f_2(r) = \sqrt{3}/2$ for all r, meaning that there is only the ψ_2 liquid. In the opposite limit $\beta_1 \to \frac{3}{16}$, we find $a_0 \to \sqrt{3}/2$ and $b_0 \to 0$. Near $r = 0$ one has the ψ_1 liquid, and for large r one finds the ψ_2 liquid. Thus, the solution is a kink-antikink interpolating between the two immiscible "liquids." Naming r_* the radius of the region where $f_1(r)$ dominates, we have $r_* \to \infty$ (the norm of ψ_1 diverges) in the strict limit $\beta_1 \to \frac{3}{16}$, with $f_1(r) \approx \psi_{cr}$ for $r \ll r_*$ and $f_1(r) \approx 0$ for $r \gg r_*$ and vice versa for $f_2(r)$.

In the following sections, we will take $\gamma = 1$. The qualitative results hold for more general values of $\gamma > 0$.
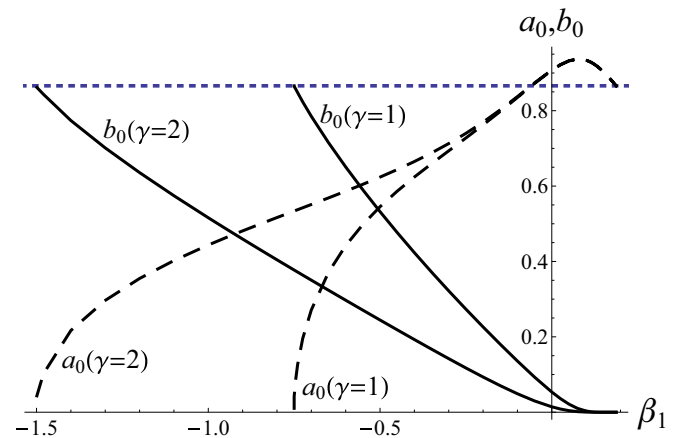
FIG. 2. (Color online) Values of $f_1(0) = a_0$ (dashed lines) and $f_2(0) = b_0$ (solid lines) computed from the numerical solutions for the families computed taking $\gamma = 1$ and $\gamma = 2$. The horizontal dotted line marks $\psi_{cr} = \sqrt{3}/2$.

III. D'ALEMBERT'S PARADOX

The so-called D'Alembert's paradox (1752) is the contradiction with observation of the mathematical solutions of the hydrodynamic equations in which an object can move within a fluid experiencing no drag. Experimentally this can only happen in superfluids. Drawing an analogy with the case at hand is useful to establish the liquid-like properties of the CQNLSE, although one should keep in mind that the equivalence is limited.

We now show that there exist solutions of Eqs. (1) in which the main bulk of the first species moves with constant velocity U within the fluid of the second species, i.e., there are situations in which the drag force is exactly zero. They correspond to steady flows in the moving reference frame. A similar behavior involving a different NLSE model was first found in Ref. [16]. Notice that we abuse of language using the word "velocity" to refer to derivatives with respect to z, which in the nonlinear optics framework correspond to propagation distance rather than time. In that case, the variations in z are a consequence of having nontrivial components of the wave vector apart from k_z and this velocity is, physically, the propagation angle with respect to the z axis. We introduce an ansatz of the form

$$\psi_1 = e^{i\,\beta_U\,z}\phi_1(x, y - Uz),$$
$$\psi_2 = e^{i\,\beta_{cr}\,z}\phi_2(x, y - Uz). \tag{6}$$

This system of equations can be treated along the lines of Ref. [26]: consider $\eta = y - Uz$ and write the system as a PDE in x, η. One finds the following:

$$iU\partial_\eta\phi_1 = \nabla^2\phi_1 + (|\phi_1|^2 - |\phi_1|^4 - \gamma|\phi_2|^2 - \beta_U)\phi_1,$$
$$iU\partial_\eta\phi_2 = \nabla^2\phi_2 + (|\phi_2|^2 - |\phi_2|^4 - \gamma|\phi_1|^2 - \beta_{cr})\phi_2, \tag{7}$$

where ∇^2 should now be understood as $\partial_x^2 + \partial_\eta^2$. Boundary conditions at infinity ($x^2 + \eta^2 \to \infty$) are $\phi_1 \to 0$, $\phi_2 \to \sqrt{3}/2$. We split real and imaginary parts as

$$\phi_1 = \phi_{1R} + i\,\phi_{1I}, \quad \phi_2 = \phi_{2R} + i\,\phi_{2I}. \tag{8}$$

The system (7) is invariant under $x \to -x$ and under $\eta \to -\eta$ together with $\phi_{1I} \to -\phi_{1I}$, $\phi_{2I} \to -\phi_{2I}$. Thus, it is enough to compute the functions for $x > 0$, $\eta > 0$ and solutions must be consistent with the following set of Neumann and Dirichlet boundary conditions at $x = 0$ and $\eta = 0$:

$$0 = \partial_x\phi_{1R}|_{x=0} = \partial_x\phi_{2R}|_{x=0} = \partial_x\phi_{1I}|_{x=0} = \partial_x\phi_{2I}|_{x=0},$$
$$0 = \partial_\eta\phi_{1R}|_{\eta=0} = \partial_\eta\phi_{2R}|_{\eta=0}, \tag{9}$$
$$0 = \phi_{1I}|_{\eta=0} = \phi_{2I}|_{\eta=0}.$$

We have found numerical solutions of the problem (7), (9) by using a finite difference method: we discretize the $x - \eta$ plane in a lattice of $N_x \times N_\eta$ points and write the resulting (approximately) $4N_xN_\eta$ algebraic nonlinear equations for the same number of real variables. Given a judicious initial ansatz, solutions can be found by a standard Newton-Raphson method. For fixed γ, there is a two-parameter family of solutions, depending on U and β_U. Since the solutions with $U = 0$ have been computed in Sec. II, they are a good starting point to search for different solutions of the family. In particular, we are interested in solutions with different U but constant
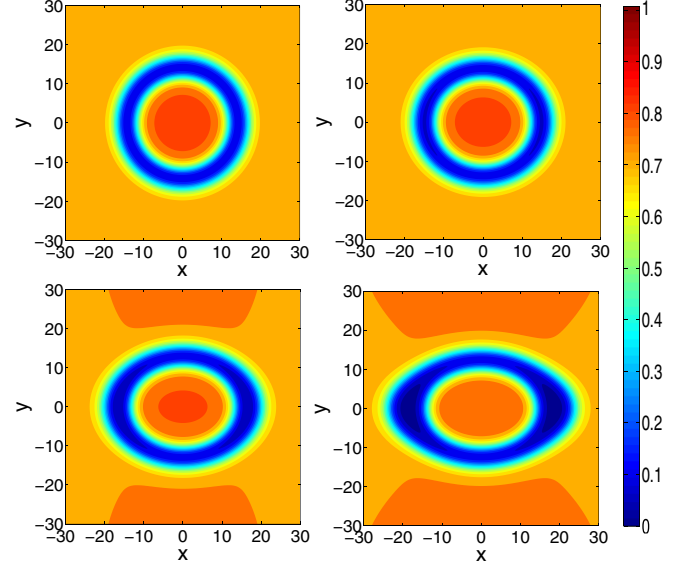
FIG. 3. (Color online) Contour plots of $|\phi_1|^2 + |\phi_2|^2$ for four solutions of Eqs. (7) with $\int |\phi_1|^2\,dx\,d\eta \approx 355$. This normalization corresponds to $\beta_1 = 0.15$ in the formalism of Sec. II. The four images correspond to $U = 0$, $U = -0.1$, $U = -0.15$, and $U = -0.17$, respectively. There is a central lump corresponding to the first species, surrounded by a region where $|\phi_1|^2 + |\phi_2|^2$ drastically diminishes and immersed in the bulk of the second species, such that, far from the center $|\phi_1|^2 + |\phi_2|^2 \to |\phi_2|^2 \to 3/4$.

$\int |\phi_1|^2\,dx\,d\eta$. The relation of β_U with the norm is nontrivial, but, for fixed U, we can vary β_U and compute different solutions until we get the one with the desired normalization. For fixed normalization, there is a maximal value of $|U|$ for which the solution exists.

A few examples of numerical approximations, computed in a 120×240 lattice, are depicted in Fig. 3. We depict contour maps of the quantity $|\phi_1|^2 + |\phi_2|^2$. It should be understood that the inner region mostly corresponds to $|\phi_1|^2$ and the outer one to $|\phi_2|^2$. The region where $|\phi_1|^2 + |\phi_2|^2$ drastically decreases is the interface. The plots show how the $|\phi_n|^2$ distributions of the traveling solutions get deformed as the velocity is increased.

It is also interesting to understand what happens if the initial conditions do not correspond exactly to these stationary solutions. With that aim, we have performed simulations in which the static solutions of Sec. II are given a boost; i.e., ψ_1 is multiplied by $e^{-i\,u_0\,y/2}$ where u_0 is (minus) the initial velocity and then used as initial conditions in (1). The evolution is computed by a standard split-step pseudospectral method, the so-called beam propagation method. In order to avoid spurious effects related to boundary conditions, we have taken a finite droplet for the second species. Simulations [28] show that, initially, the boosted soliton loses momentum to the medium but eventually tends to a constant velocity, approaching the above described behavior related to D'Alembert's paradox.

In order to describe this effect quantitatively, let us define the central position of the ψ_1 droplet as

$$\langle y_1 \rangle(z) = \frac{\int \int y|\psi_1(z)|^2\,dx\,dy}{\int \int |\psi_1(z)|^2\,dx\,dy} \tag{10}$$
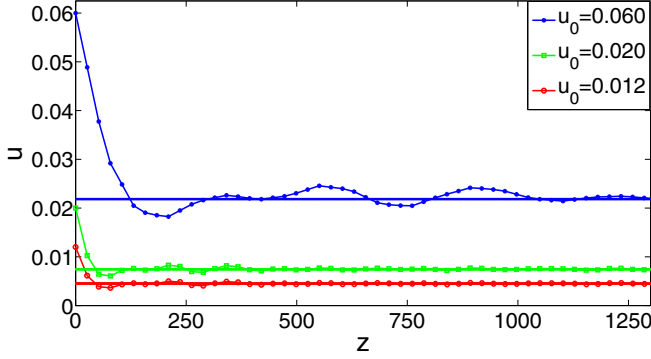
FIG. 4. (Color online) Examples of the evolution with z of the velocity of the first species main bulk immersed in the dragging fluid. The horizontal lines mark the asymptotic velocity inferred from the simulations. Larger values of u_0 yield larger asymptotic values of $u(z)$.

and its velocity as $u(z) = -\frac{d\langle y_1 \rangle(z)}{dz}$. Figure 4 shows how u evolves upon propagation for different examples.

IV. TERMINAL VELOCITY AND DRAG FORCE

We now devise a thought experiment which can be considered an NLSE version of the evolution of a body moving within a fluid subject to an external force. Let us modify (1) to include an extra term accounting for a potential acting on ψ_1 along the y direction, which in the case of optics would correspond to a linear variation of the linear refractive index:

$$-i\partial_z \psi_1 = \nabla^2 \psi_1 + (|\psi_1|^2 - |\psi_1|^4 - \gamma |\psi_2|^2)\psi_1 - g\,y\,\psi_1,$$

$$-i\partial_z \psi_2 = \nabla^2 \psi_2 + (|\psi_2|^2 - |\psi_2|^4 - \gamma |\psi_1|^2)\psi_2. \quad (11)$$

We will consider an initially static solution as discussed in Sec. II, for which g is eventually turned on, namely, $g = 0$ for $z < 0$ and is shifted to a constant for $z > 0$. We compute this evolution by numerically integrating (4) by the split-step pseudospectral beam propagation method. The ψ_1 distribution starts drifting driven by g, but the drag force of the fluid eventually stops the acceleration and the motion tends to a terminal velocity $u_T(g)$.

The qualitative behavior is different for small and large g. For large g, a void is generated in the wake of the moving object. For smaller g, vortex-antivortex pairs get detached from this void, contributing to the drag force. This behavior is parallel to the one described in Ref. [7] for the case in which a superfluid modeled by a cubic-quintic equation flows past a rigid obstacle. It is worth mentioning that the confluence of the liquid which isolates the vortex and antivortex from the void generated by the moving object qualitatively resembles a splash singularity [27], even if the mathematical details are rather different.

Notice that, as also happened in the setup of Sec. III, the initially round ψ_1 distribution gets somewhat deformed. As it could be expected, the deformation is greater when larger velocities are reached. Moreover, for large velocities, the surface tension forces of the surrounding liquid fail to rapidly occupy the void left at the object's trail and a bubble is
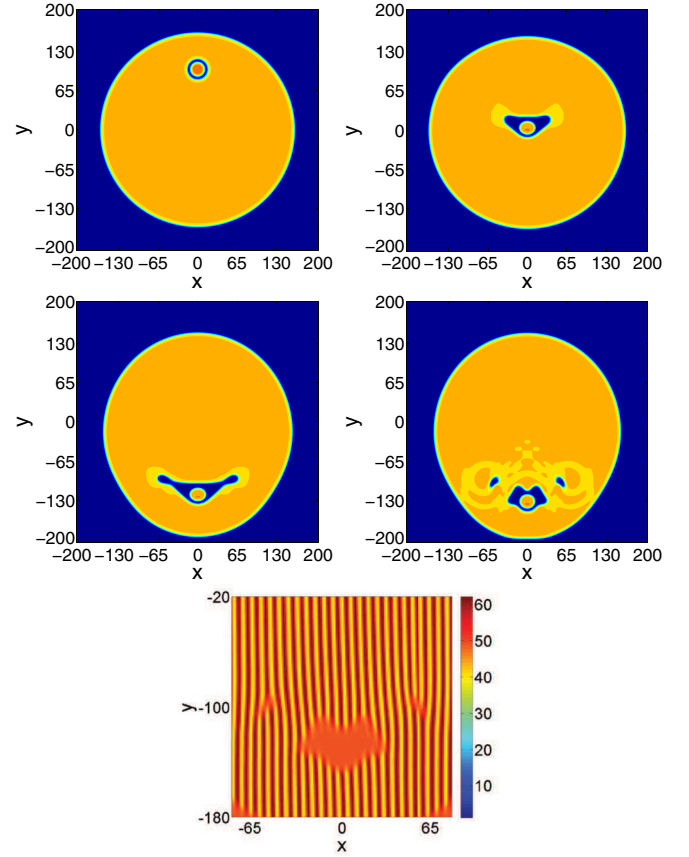
FIG. 5. (Color online) Evolution with $g = 8 \times 10^{-4}$. The initial configuration is the static solution with $\beta_1 = 0.15$. The four first images correspond to $z = 0$, 800, 1900, and 2000, respectively, and their color convention is as in Fig. 3. A little droplet of the first species moves within a large but finite drop of the second one ($|\psi_1|^2 + |\psi_2|^2 \to 0$ as $r \to \infty$). The terminal velocity is moderate, and the moving object leaves a trail of vortex-antivortex pairs (shown in the figure as regions with small $|\psi_1|^2 + |\psi_2|^2$), whose nucleation and detachment contribute to the drag force. The plot below explicitly shows the phase singularities of the vortex and antivortex, which appear as forklike structures in the interference pattern of the wave function with a plane wave. Concretely, the image corresponds to $|\psi_2(z = 2000) + 7 \exp(1000\,i\,x)|^2$.

generated. Figures 5 and 6 show representative examples see also Ref. [28].

In this setup, it is possible to compute numerically the terminal velocity for different values of g and different initial functions ψ_1, corresponding to different values of β_1 as defined in Sec. II. We restrict ourselves to values of β_1 not far from β_{cr} in order to have distributions of ψ_1 for which the analogy to a body within a fluid is applicable to some extent. We plot some results in Fig. 7.

As $g \to 0$ the value of u_T tends to a positive constant, as it could be expected from the D'Alembert's paradox behavior. This result is reminiscent of Ref. [16], even if the setup is rather different. For large values of g, the drag becomes quadratic in velocity. When β_1 is very near β_{cr}, the quadratic drag regime already starts at small velocities. Presumably, the reason is that the lump becomes more malleable in this regime yielding a modification of the qualitative behavior.
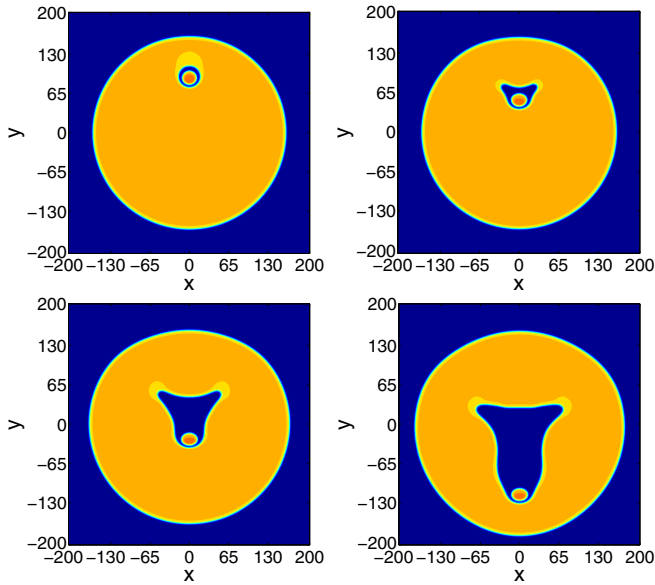
FIG. 6. (Color online) Evolution with $g = 2 \times 10^{-3}$. The four images correspond to $z = 100, 300, 600,$ and 900, respectively. Colors are as in Fig. 3. The terminal velocity is larger than in the previous case, and the advance of the main bulk of the first species leaves a bubble at its wake.

For certain ranges of g and different values of β_1, the results can be approximated by straight lines (notice, however, that for small g, u_T can decrease with increasing g). This linear growth suggests the possibility of considering a simple modeling of the situation in which the drag force is just considered linear in velocity. A body subject to a constant force and a quadratic drag force satisfies $\frac{d\langle y_1 \rangle}{dz} = -g + k\,u$, which gives $\langle y_1 \rangle = -\frac{g}{k^2}(k\,z + e^{-k\,z} - 1)$. We have compared the numerically computed trajectories $\langle y_1(z) \rangle$ to fits of the form

$$\langle y_1(z) \rangle = -a(b\,z + e^{-b\,z} - 1), \tag{12}$$

where a and b are taken as free parameters. It turns out that the simple mechanical model is rather precise for the setup of the present section in a large range of parameters. This cannot be an exact characterization of the system for several reasons: first, we have seen in Sec. III that there are dragless flows and (12)
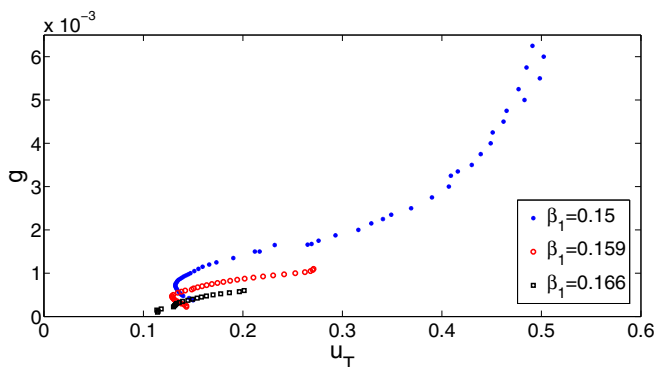
FIG. 7. (Color online) Some examples of $g(u_T)$.
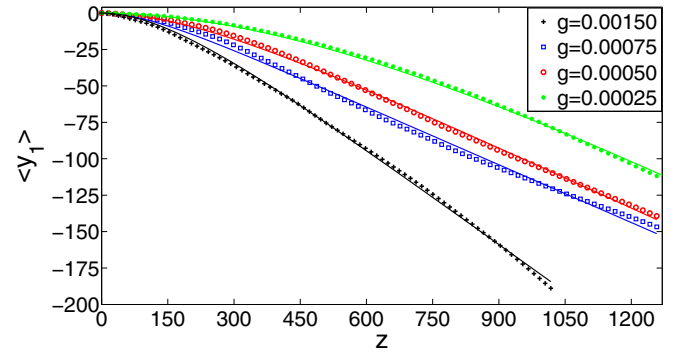
FIG. 8. (Color online) Examples of comparison of $\langle y_1(z) \rangle$ computed numerically (dots) with fits to the simple model (12) (solid lines). In all cases the initial conditions use the $\beta_1 = 0.15$ solution of Sec. II. As it could be expected, for greater values of g, the displacement $\langle y_1(z) \rangle$ is larger.

fails to describe them. Indeed, a more complicated dependence of the drag force on u was found in Fig. 7, which could be introduced in the mechanical model at the cost of losing simplicity. Moreover, since the "object" itself gets deformed while propagating, its interaction with the environment should depend on its form too. This explains, for instance, the mild oscillations of the simulated motion in Fig. 8 around the solid lines. As the β_1 of the initial distribution deviates away from β_{cr}, the precision of the simple modeling (12) declines.
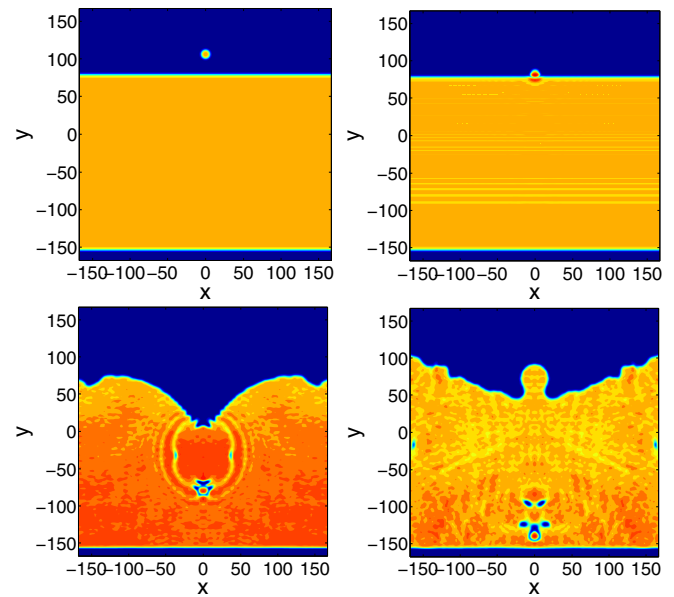
FIG. 9. (Color online) A soliton entering the bulk of a fluid, as described by a bimodal system of cubic-quintic nonlinear Schrödinger equations. The different images correspond to $z = 10, 50, 500, 700$ in the simulation. Colors are as in Fig. 3. In the last image, six bubbles [blue (dark gray) spots] inside the liquid and separated from the wake of the object can be observed. The four at the object's trail correspond to two vortex-antivortex pairs. The two small ones by the vertical edges of the figure are rarefaction pulses, namely, dark traveling waves without vorticity.

V. INITIALLY SEPARATED SPECIES

Up to now we have considered situations in which species 1 is initially within the fluid. In this section we illustrate the case in which both species are separated at the outset, while afterwards the soliton of species 1 enters the bulk of species 2. Concretely, we consider Eqs. (1) with a linear potential term $-g\,y\,\psi_n$ for both species. For species 2, we also include a potential barrier at the bottom. Periodic boundary conditions are considered in the x direction. The evolution is depicted in Fig. 9; see also Ref. [28].

We observe that the collision produces surface and body waves. Due to the analogy to a system with surface tension of the cubic-quintic equations, the behavior at the surface resembles that of a liquid hit by an object. Once the soliton enters the liquid, it starts experiencing a drag force as described in the previous sections. The simulation shows the eventual nucleation of vortex-antivortex pairs related to this friction process; see the last image in Fig. 9. Moreover, since the liquid is somewhat stirred, dark solitary traveling waves (namely, rarefaction pulses [9,26]) can be excited. Two of them moving horizontally in opposite directions can be seen in the plots.

VI. CONCLUSIONS

We have analyzed a coupled system of cubic-quintic nonlinear Schrödinger equations in order to understand drag forces in physical systems that can be modeled as fluids within this formalism, such as the so-called liquid light or certain Bose-Einstein condensates. The two equations correspond to having two modes, such as transverse polarizations for light or different atomic species. A concentrated distribution of one of the species immersed in a larger fluid of the other one is subject to macroscopic forces that influence its dynamics. For small velocities, there are situations in which a D'Alembert's paradox situation exists, namely, the lump moves preserving its form and velocity. Notice, however, that it would be wrong to say that it is unaffected by the inviscid fluid, since the energy distribution of the first species does depend on its velocity, as shown in Fig. 3. For larger velocities, the drag forces set in. Roughly, it can be said that they grow linearly with u in a certain region and then grow quadratically for larger u. It is possible to establish an approximate mechanical analogy and consider that the system is just described by a simple equation for a rigid object subject to a force which only depends on velocity. This modeling is accurate to some extent but it is obviously limited since, for instance, it disregards deformations of both the fluid and the object as described by the CQNLSEs, which also alter the macroscopic dynamics. Overall, these results give further evidence of the qualitative resemblance of physical systems modeled by the CQNLSE to ideal liquids.

ACKNOWLEDGMENTS

[1] F. Dalfovo, S. Giorgini, L. P. Pitaevskii, and S. Stringari, Rev. Mod. Phys. **71**, 463 (1999).

[2] G. P. Agrawal, *Nonlinear Fiber Optics*, 4th ed. (Elsevier/Academic Press, New York, 2006).

[3] Y. S. Kivshar and B. Luther-Davies, Phys. Rep. **298**, 81 (1998).

[4] J. Herrmann, Opt. Commun. **91**, 337 (1992); F. G. Bass, V. V. Konotop, and S. A. Puzenko, Phys. Rev. A **46**, 4185 (1992); W. Królikowski, N. Akhmediev, and B. Luther-Davies, Phys. Rev. E **48**, 3980 (1993).

[5] A. H. Piekara, J. S. Moore, and M. S. Feldt, Phys. Rev. A **9**, 1403 (1974).

[6] I. V. Barashenkov and E. Y. Panova, Physica D **69**, 114 (1993); C. Josserand and S. Rica, Phys. Rev. Lett. **78**, 1215 (1997); T. A. Davydova, A. I. Yakimenko, and Yu. A. Zaliznyak, Phys. Rev. E **67**, 026402 (2003); B. B. Baizakov, A. Bouketir, A. Messikh, A. Benseghir, and B. A. Umarov, Int. J. Mod. Phys. B **25**, 2427 (2011); R. M. Caplan, R. Carretero-Gonzalez, R. Kevrekidis, and B. A. Malomed, Math. Comp. Simul. **82**, 1150 (2012); C. Trallero-Giner, R. Cipolatti, and T. C. H. Liew, Eur. Phys. J. D **67**, 143 (2013).

[7] C. Josserand, Y. Pomeau, and S. Rica, Phys. Rev. Lett. **75**, 3150 (1995).

[8] V. Prytula, V. Vekslerchik, and V. M. Pérez-García, Phys. Rev. E **78**, 027601 (2008).

[9] A. Paredes, D. Feijoo, and H. Michinel, Phys. Rev. Lett. **112**, 173901 (2014).

[10] K. Dimitrevski *et al.*, Phys. Lett. A **248**, 369 (1998); V. I. Berezhiani, V. Skarka, and N. B. Aleksic, Phys. Rev. E **64**, 057601 (2001); R. L. Pego and H. A. Warchall, J. Nonlinear Sci. **12**, 347 (2002); H. Michinel, J. R. Salgueiro, and M. J. Paz-Alonso, Phys. Rev. E **70**, 066605 (2004).

[11] W. Chang, A. Ankiewicz, J. M. Soto-Crespo, and N. Akhmediev, Phys. Rev. A **78**, 023830 (2008).

[12] D. E. Edmundson and R. H. Enns, Phys. Rev. A **51**, 2491 (1995); M. Quiroga-Teixeiro and H. Michinel, J. Opt. Soc. Am. B **14**, 2004 (1997); D. Mihalache, D. Mazilu, L.-C. Crasovan, I. Towers, A. V. Buryak, B. A. Malomed, L. Torner, J. P. Torres, and F. Lederer, Phys. Rev. Lett. **88**, 073902 (2002); H. Michinel, J. Campo-Táboas, R. García-Fernández, J. R. Salgueiro, and M. L. Quiroga-Teixeiro, Phys. Rev. E **65**, 066604 (2002); M. J. Paz-Alonso, D. Olivieri, H. Michinel, and J. R. Salgueiro, *ibid.* **69**, 056601 (2004).

[13] D. Novoa, H. Michinel, and D. Tommasini, Phys. Rev. Lett. **103**, 023903 (2009).

[14] Z. Wu, Y. Zhang, C. Yuan, F. Wen, H. Zheng, Y. Zhang, and M. Xiao, Phys. Rev. A **88**, 063828 (2013).

[15] H. Michinel, M. J. Paz-Alonso, and V. M. Pérez-García, Phys. Rev. Lett. **96**, 023903 (2006); A. Alexandrescu, H.

Michinel, and V. M. Pérez-García, Phys. Rev. A **79**, 013833 (2009).

[16] T. Frisch, Y. Pomeau, and S. Rica, Phys. Rev. Lett. **69**, 1644 (1992).

[17] S. V. Manakov, Zh. Eksp. Teor. Fiz. **65**, 505 (1973) [Sov. Phys. JETP **38**, 248 (1974)].

[18] G. Modugno, M. Modugno, F. Riboli, G. Roati, and M. Inguscio, Phys. Rev. Lett. **89**, 190404 (2002).

[19] C. J. Myatt, E. A. Burt, R. W. Ghrist, E. A. Cornell, and C. E. Wieman, Phys. Rev. Lett. **78**, 586 (1997).

[20] X. Liu, H. Pu, B. Xiong, W. M. Liu, and J. Gong, Phys. Rev. A **79**, 013423 (2009); G. Csire, D. Schumayer, and B. Apagyi, *ibid.* **82**, 063608 (2010); Z. M. He, D. L. Wang, J. W. Ding, and X. H. Yan, Eur. Phys. J. D **66**, 139 (2012); D. Feijoo, A. Paredes, and H. Michinel, Phys. Rev. A **87**, 063619 (2013).

[21] A. Maimistov, B. Malomed, and A. Desyatnikov, Phys. Lett. A **254**, 179 (1999).

[22] D. Mihalache, D. Mazilu, I. Towers, B. A. Malomed, and F. Lederer, J. Opt. A **4**, 615 (2002); Phys. Rev. E **67**, 056608 (2003); D. Mihalache, D. Mazilu, B. A. Malomed, and F.

Lederer, J. Opt. B **6**, S341 (2004); A. S. Desyatnikov, D. Mihalache, D. Mazilu, B. A. Malomed, C. Denz, and F. Lederer, Phys. Rev. E **71**, 026615 (2005); J. M. Alcaraz-Pelegrina and P. Rodriguez-Garcia, Phys. Lett. A **374**, 1591 (2010); P. Wang and B. Tian, Opt. Commun. **285**, 3567 (2012).

[23] P. Wang and B. Tian, J. Mod. Opt. **59**, 1786 (2012).

[24] J. M. Alcaraz-Pelegrina and P. Rodriguez-Garcia, Phys. Lett. A **375**, 2815 (2011).

[25] B. B. Baizakov, A. Bouketir, A. Messikh, and B. A. Umarov, Phys. Rev. E **79**, 046605 (2009).

[26] C. A. Jones and P. H. Roberts, J. Phys. A **15**, 2599 (1982); C. A. Jones, S. J. Putterman, and P. H. Roberts, *ibid.* **19**, 2991 (1986); D. Chiron and C. Scheid, preprint, HAL-Inria Open Archive hal-00873794, http://hal.archives-ouvertes.fr/docs/00/87/37/94/PDF/Endim2.pdf.

[27] A. Castro, D. Córdoba, C. L. Fefferman, F. Gancedo, and J. Gómez-Serrano, Proc. Natl. Acad. Sci. USA **109**, 733 (2012).

[28] See Supplemental Material at http://link.aps.org/supplemental/10.1103/PhysRevE.90.033204 for animations of several simulations.